46. The same is found for benthic $\delta^{18}O$. We present the planktonic record because it has better coherence with orbital precession and with the lithogenic % and flux records. Carbonate dissolution prevents development of a continuous $\delta^{18}O$ record (*G. sacculifer*) from 2.85 to 3.5 Ma. However, lithogenic % and $\delta^{18}O$ data (*G. sacculifer*) over the intervals 3.4 to 3.73 Ma and 4.2 to 4.5 Ma indicate in-phase relations.
47. S. C. Clemens and W. L. Prell, in *Proc. ODP Sci. Results*, W. L. Prell, N. Niitsuma, P. A. Meyers, K.-C. Emeis, Eds. (Ocean Drilling Program, College Station, TX, 1991), vol. 117, pp. 365–388.
48. J. E. Kutzbach and P. J. Guetter, *J. Atmos. Sci.* **43**, 1726 (1986).
49. W. L. Prell and J. E. Kutzbach, *Nature* **360**, 647 (1992).
50. P. B. deMenocal and D. Rind, *J. Geophys. Res.* **98**, 7265 (1993).
51. T. E. Cerling, J. R. Bowman, J. R. O'Neil, *Palaeogeogr. Palaeoclimatol. Palaeoecol.* **63**, 335 (1988).
52. F. A. Street-Perrott, J. F. B. Mitchell, D. S. Marchand, J. S. Btunner, *Trans. R. Soc. Edinburgh Earth Sci.* **81**, 407 (1990).
53. G. B. Bonan, D. Pollard, S. L. Thompson, *Nature* **359**, 716 (1992).
54. J. A. Foley, J. E. Kutzbach, M. T. Coe, S. Levis, *ibid.* **371**, 52 (1994).
55. N. J. Shackleton, S. Crowhurst, T. Hagleberg, N. G. Pisias, D. A. Schneider, in *Proc. ODP Sci. Results* (Ocean Drilling Program, College Station, TX, 1995), vol. 138, p. 73–101.
56. K.-C. Emeis, D. M. Anderson, H. Doose, D. Kroon, D. Schulz-Bull, *Quat. Res.* **43**, 355 (1995).
57. M. A. Altabet, R. Francois, D. W. Murray, W. L. Prell, *Nature* **373**, 506 (1995).
58. P. Schafer and V. Ittekkot, *Naturwissenschaften* **80**, 511 (1993).
59. R. A. Mortlock and P. N. Froelich, *Deep-Sea Res.* **36**, 1415 (1989).
60. J. W. Farrell and T. R. Janecek, in *Proc. ODP Sci. Results*, J. Peirce and J. Weissel, Eds. (Ocean Drilling Program, College Station, TX, 1991), vol. 121, pp. 297–355.
61. G. M. Jenkins and D. G. Watts, *Spectral Analysis and Its Applications* (Holden Day, Oakland, 1968).
62. Supported by the Ocean Science Division of the NSF and JOI/USSSP. Samples were provided by the international Ocean Drilling Program. Technical assistance was provided by L. Nik, J. Cook, and A. Martin. We thank F. Sirocko and R. Tiedemann for valuable comments and constructive criticisms.

2 July 1996; accepted 13 September 1996

Structure of the MDM2 Oncoprotein Bound to the p53 Tumor Suppressor Transactivation Domain

Paul H. Kussie, Svetlana Gorina, Vincent Marechal, Brian Elenbaas, Jacque Moreau, Arnold J. Levine, Nikola P. Pavletich*

The MDM2 oncoprotein is a cellular inhibitor of the p53 tumor suppressor in that it can bind the transactivation domain of p53 and downregulate its ability to activate transcription. In certain cancers, MDM2 amplification is a common event and contributes to the inactivation of p53. The crystal structure of the 109-residue amino-terminal domain of MDM2 bound to a 15-residue transactivation domain peptide of p53 revealed that MDM2 has a deep hydrophobic cleft on which the p53 peptide binds as an amphipathic α helix. The interface relies on the steric complementarity between the MDM2 cleft and the hydrophobic face of the p53 α helix and, in particular, on a triad of p53 amino acids—Phe^{19}, Trp^{23}, and Leu^{26}—which insert deep into the MDM2 cleft. These same p53 residues are also involved in transactivation, supporting the hypothesis that MDM2 inactivates p53 by concealing its transactivation domain. The structure also suggests that the amphipathic α helix may be a common structural motif in the binding of a diverse family of transactivation factors to the TATA-binding protein–associated factors.

The p53 tumor suppressor helps maintain the genomic integrity of the cell as it coordinates the cellular response to DNA damage by inducing cell cycle arrest (*1*) or apoptosis (*2*, *3*). Accordingly, inactivation of p53 is one of the most common events in neoplastic transformation. In about half of all cancer cases, p53 is inactivated by mutations and other genomic alterations (*4*), and in many of the remaining cases it is functionally inactivated by the binding of the cellular MDM2 oncoprotein, which was originally identified as an amplified gene in a transformed mouse cell line (*5–7*).

p53 can bind to specific DNA sequences (*8*) and activate gene expression (*9*), and this activity of p53 is likely to be central to its growth and suppressing effects because tumor-derived mutants are defective in DNA binding (*8–10*). In normal cells, MDM2 and p53 form a negative feedback loop that helps to limit the growth-suppressing activity of p53 (*11*). In response to DNA damage, which leads to an increase in p53 (*1*), p53 can activate expression of the MDM2 gene (*11*). The MDM2 protein, in turn, can bind the transactivation domain of p53, inhibiting further p53 activity as a transcription factor (*6*, *11*, *12*). Deletion of MDM2 is lethal to mouse embryos, but transgenic mice lacking both MDM2 and p53 are viable (*13*), suggesting that the downregulation of the growth-suppressing effects of p53 is a key activity of MDM2.

In tumors, gene amplifications and other alterations can result in elevated MDM2 and lead to the constitutive inhibition of p53. Amplification of MDM2 has been observed in more than one-third of soft tissue sarcomas (*7*, *14*) and, less often, in other cancers, including glioblastomas (*15*), leukemias (*16*), esophageal carcinomas (*17*), and breast carcinomas (*18*). Tumors harbor-

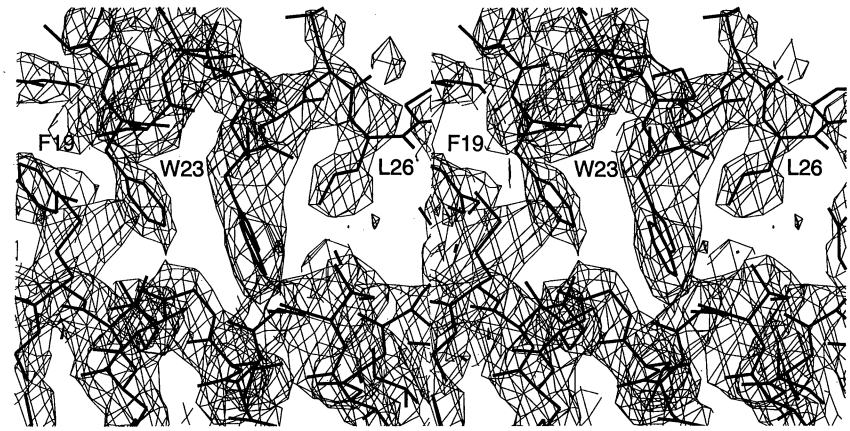

Fig. 1. MIR electron density map of the *X. laevis* MDM2-p53 interface at 3.0 Å resolution, contoured at 1.0 σ, with the refined 2.3 Å resolution atomic model in a stick representation. Stereo view focuses on the interactions of Phe^{19}, Trp^{23}, and Leu^{26} of p53 (labeled) with the α2 helix of MDM2.

P. H. Kussie, S. Gorina, and N. P. Pavletich are with the Cellular Biochemistry and Biophysics Program, Memorial Sloan-Kettering Cancer Center, New York, NY 10021, USA.
V. Marechal is with the Cervice de Microbiologie, Hopital Rothschild, F-75571, Paris 12, France.
B. Elenbaas and A. J. Levine are in the Department of Molecular Biology, Princeton University, Princeton, NJ 08544, USA.
J. Moreau is at the Institut Jacque Monad, Equipe d'Embryologie, 75251, Paris, France.

*To whom correspondence should be addressed. E-mail: nikola@xray2.mskcc.org

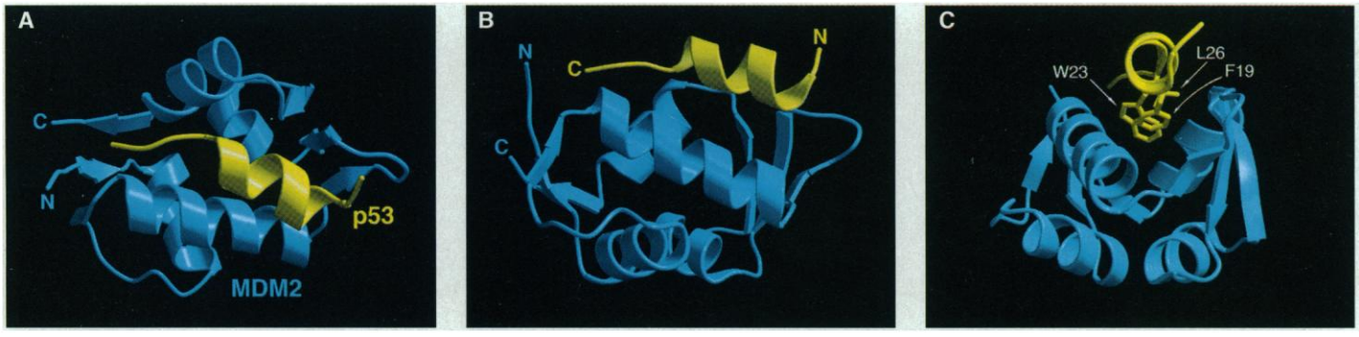

Fig. 2. The MDM2 NH_2-terminal domain (in cyan) forms a structure reminiscent of a twisted trough. It has a hydrophobic cleft where the p53 peptide (in yellow) binds as an amphipathic α helix. Three approximately orthogonal views of the complex are shown. (**A**) The MDM2-p53 complex in an orientation where the floor of the MDM2 cleft is in the plane of the figure. MDM2, p53 and the NH_2- and COOH-termini are labeled C and N. (**B**) The complex rotated approximately 90° about the horizontal axis of (A). (**C**) The complex rotated approximately 90° about the vertical axis of (B), looking down the helix axis of p53. Also shown are Phe^{19}, Trp^{23}, and Leu^{26} of p53, which insert deep into the MDM2 cleft [prepared with the programs MOLSCRIPT (*50*) and RASTER3D (*51*)]. Abbreviations for the amino acid residues are: A, Ala; C, Cys; D, Asp; E, Glu; F, Phe; G, Gly; H, His; I, Ile; K, Lys; L, Leu; M, Met; N, Asn; P, Pro; Q, Gln; R, Arg; S, Ser; T, Thr; V, Val; W, Trp; Y, Tyr.

ing amplified MDM2 typically contain wild-type p53 (*7*, *14*), suggesting that MDM2 amplification may be an alternative to the mutational inactivation of p53 in tumorigenesis. This hypothesis is supported by the ability of MDM2 to enhance the tumorigenic potential of cells (*19*) and transform them in cooperation with activated *ras* (*20*).

We now describe the crystal structure of the 109-amino-acid NH_2-terminal domain of MDM2, which contains the p53 binding activity (*12*, *21*), bound to a peptide from the transactivation domain of p53. The structure reveals how the transactivation domain of p53 binds MDM2, and in conjunction with the crystal structure of the p53 DNA-binding domain–DNA complex (*22*) and structures of the p53 oligomerization domain (*23*), help to elucidate how p53 functions as a transcription factor.

Structure determination. The approximate boundaries of the interacting regions of MDM2 and p53 had been identified by a combination of deletion and mutation analyses (*12*, *21*, *24*, *25*). In this study, proteolytic digestion was used for the more precise delineation of the boundaries of the interacting regions (*26*). This analysis showed that MDM2 contains a 12-kD structural domain at its NH_2-terminal portion [residues 17 to 125 (*26*)] that is highly conserved (71 to 91 percent identity across five species) and is necessary and sufficient for p53 binding; on the part of p53, MDM2 binding depends on a short, linear sequence of 11 amino acids [residues 17 to 27 (*26*)] including the residues identified by mutagenesis as being necessary for MDM2 binding (*24*, *25*). This region also overlaps one of the conserved regions of p53 (*3*) and contains sequences responsible for transactivation (*9*, *12*, *21*).

In crystallization trials, 15- and 17-residue p53 peptides produced crystals of the complex, but larger ones did not, presumably because their ends are likely to extend beyond the boundaries of the MDM2 cleft in the complex, thus interfering with crystal packing. Initial isothermal titration calorimetry experiments showed that the crystallization peptides have an affinity for MDM2 comparable to that of a larger p53 peptide, encompassing the region previously identified as sufficient for MDM2 binding (*12*) (apparent dissociation constants (K_d) of 600 nM and 420 nM for peptides corresponding to residues 15 to 29 and 1 to 57 of p53, respectively, at 35°C). Crystals of the human MDM2 (residues 17 to 125)–p53 (residues 15 to 29) complex grew as tightly clustered thin plates, and successive rounds of macroseeding were required to obtain single crystals suitable for diffraction (*27*). To circumvent this problem, crystals of *Xenopus laevis* MDM2 [residues 13 to 118; 71 percent identity to human MDM2 (*28*)] bound to human p53 (residues 13 to 29), which grew readily, were used for the structure determination by the multiple isomorphous replacement (MIR) method (Fig. 1 and Table 1) (*29*). The structure of the human MDM2-p53 complex was then determined by molecular replacement using the 2.3 Å structure of the X. *laevis* complex (*R* factor of 18.8 percent) as a model, and it was refined at 2.6 Å resolution to an *R* factor of 20.0 percent (Table 1) (*29*).

Table 1. Statistics from the crystallographic analysis.

Data set	Resolution (Å)	Reflections		Data coverage (%)	R_{sym}*	MFID†	Phasing power‡
		Measured	Unique				
Native (*X. laevis*)	2.3	15953	6257	97.0	0.055		
Native (human)	2.6	16069	3559	90.0	0.052		
Thimerosal	3.0	6707	2886	94.8	0.056	0.25	1.9
$UO_2(OAc)_2$	3.1	6039	2545	93.2	0.078	0.12	1.4
$UO_2(OAc)_2 + K_2Pt(CN)_4$	3.2	14350	2181	86.9	0.088	0.16	1.8
$K_2Au(CN)_4$	3.0	4316	2592	86.4	0.024	0.08	0.8

Refinement statistics

	Resolution (Å)	Reflections§	Protein atoms	Water atoms	*R*‖	R_{free}¶	rmsd#		
							Bonds (Å)	Angles (°)	*B* factors (Å²)
X. laevis	7.0–2.3	5423	801	40	0.188	0.253	0.010	1.39	3.1
Human	8.0–2.6	3293	807		0.200	0.276	0.013	1.55	2.7

*$R_{sym} = \Sigma_h\Sigma_i|I_{h,i} - I_h|/\Sigma_h\Sigma_i I_{h,i}$ for the intensity (*I*) of *i* observations of reflection *h*. †MFID, mean isomorphous difference = $\Sigma|F_{PH} - F_P|/\Sigma F_{PH}$, where F_{PH} and F_P are the derivative and native structure factors, respectively. ‡Phasing power = $\{[F_{H(c)}^2/(F_{PH(o)} - F_{PH(c)})^2\}^{1/2}$. §Reflections with $|F|>2\sigma$ and $|F|>1\sigma$ for the data sets from *X. laevis* and humans, respectively. ‖*R* factor = $\Sigma||F_o| - |F_c||/\Sigma|F_o|$, where F_o and F_c are the observed and calculated structure factors, respectively. ¶Free *R* factor calculated from 10 percent of the data chosen randomly and omitted from simulated annealing refinement from 3000 K. #Root-mean-square deviations from ideal geometry and root-mean-square variation in the *B* factors of bonded atoms.

Overall structure of the MDM2-p53 complex. The MDM2 NH_2-terminal domain forms a structure reminiscent of a twisted trough, having a cleft lined with hydrophobic amino acids (Fig. 2). The cleft is composed of two helices forming the sides, two shorter helices that make up the bottom, and a pair of three-stranded β sheets that cap each end (Fig. 2A). The p53 peptide forms an amphipathic α helix of about 2.5 turns (Fig. 2), which is followed by an extended region of three residues. The primary contacts from p53 are made by its α helix, which binds the MDM2 cleft with its hydrophobic face and buries all but one of its five hydrophobic amino acids at the interface.

The key to the interface is a triad of hydrophobic and aromatic amino acids of p53—Phe^{19}, Trp^{23}, and Leu^{26}—which inserts deep into the MDM2 cleft (Fig. 2C). These amino acids are invariant across species (*24*). The interface relies extensively on van der Waals contacts and the steric complementarity between the MDM2 cleft and the hydrophobic face of the p53 helix as these interactions are augmented by only two intermolecular hydrogen bonds.

The structure, in conjunction with biochemical studies, reveals the mechanism of p53 inhibition by MDM2. Mutagenesis studies have implicated several hydrophobic amino acids on the amphipathic helix of p53 in transactivation (*24*), probably because of their binding to the TATA box-binding protein-associated factors (TAFs) (*30*). MDM2 makes extensive contacts to these hydrophobic p53 residues, shielding them from the solvent and preventing their access to the TAFs.

Structure of MDM2. The MDM2 domain contains a structural repetition. It has two portions, 45 and 38 amino acids long, with similar structures (residues 26 to 70 and 71 to 108) that are related by an approximate dyed axis of symmetry (Figs. 2A and 3). The sequence similarity of the two halves is low (11 percent identity), except for a general conservation of hydrophobic residues. The repeat structure consists sequentially of a β strand, an α helix, a β strand, a longer α helix, and a β strand (Fig. 3). The two helices of the repeat, which pack at an angle of ~70°, and the first two β strands, which form a β sheet, come together to form a small globular structure with a hydrophobic core.

One side of this globular repeat structure is hydrophobic, and the two repeats come together and pack across their hydrophobic sides forming a cleft at their interface (Fig. 2). Their short helices (α1 and α1′) pack in an antiparallel fashion to form the bottom of the cleft, their long helices (α2 and α2′) form the sides of the cleft, and their β strands form two β sheets at opposite ends of the cleft that cap the ends (Figs. 2 and 3). One β sheet contains the NH_2- and COOH-termini of the polypeptide, and we refer to it as the terminal β sheet to distinguish it from the β sheet that occurs in the middle of the polypeptide (middle β sheet). The cleft is about 25 Å long, 10 Å wide near the surface but narrowing toward the bottom, and up to 10 Å deep. The cleft has two layers of hydrophobic amino acids. One layer forms a hydrophobic core that seals the bottom of the cleft and an additional layer forms the hydrophobic lining of the cleft.

Although the two repeats have similar tertiary structures, the MDM2 cleft is asymmetric. One portion, which corresponds to about three-quarters of the length of the cleft and is the site where the p53 α helix makes its primary contacts, resembles a

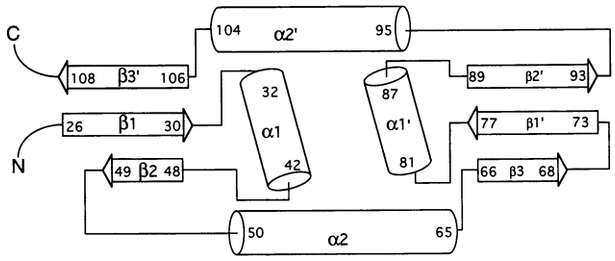

Fig. 3. The MDM2 NH_2-terminal domain contains two structurally similar portions related by an approximate dyad axis of pseudosymmetry. In this topological diagram of the secondary structure elements of MDM2, the residues at the start and the end of each secondary structure element are indicated. The structural elements of the second repeat are distinguished from those of the first repeat by the 'prime' symbol.

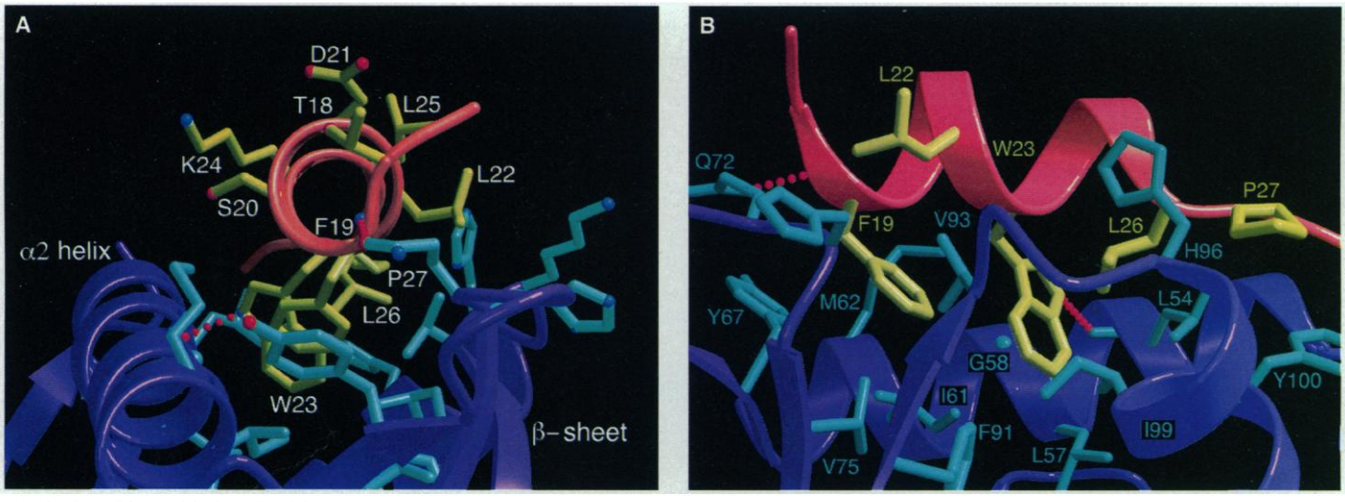

Fig. 4. The p53 peptide (in yellow) forms an amphipathic helix whose hydrophobic face binds the MDM2 cleft (in blue). The cleft is formed by the α2 helix, on one side, and the middle β sheet, on the other side, and is lined with hydrophobic and aromatic amino acids (or both). (**A**) The helical p53 amino acids show and emphasize the amphipathic nature of the α helix, where blue and red spheres indicate nitrogen and oxygen atoms, respectively, and the carbon atoms are in yellow. View is looking down the helix axis, as in Fig. 2C. For simplicity, only the p53 amino acids are labeled, although the MDM2 amino acids at the interface are also shown. The backbone regions of p53 and MDM2 are colored in a darker tone, and the two intermolecular hydrogen bonds at the interface are shown as red dotted lines. (**B**) The interface in an orientation rotated 90° about the vertical axis of (A). The MDM2 α2 helix is below the plane of the figure, its β sheet is above the plane, and p53 is between the two. Only the interacting amino acids at the interface are shown, and they are labeled.

wide, deep pocket. The remaining portion, where the extended region of p53 makes only a few contacts, is narrower and shallower, and offers a smaller interaction area with little hydrophobic character. The asymmetry in the cleft results, in part, from the α2 helix in the first repeat being about one turn longer than the corresponding α2′ helix in the second repeat, and the middle β sheet being larger than the terminal β sheet at the other end of the cleft (Figs. 2 and 3).

Structure of the p53 peptide. The p53 peptide used in the crystallization is 15 amino acids long (residues 15 to 29), but only 13 amino acids (residues 17 to 29) are ordered in the crystals. Residues 18 to 26 form an amphipathic α helix (Fig. 4A), and residues 17 and 27 to 29 at either end are in extended conformations (Fig. 4). The helix is a regular α helix until its COOH-terminal portion where it makes one 3_{10} helical hydrogen bond.

Contributing to the initiation of the α helix is a network of hydrogen bonds formed by the Thr^{18} and Asp^{21} residues. The Thr^{18} side-chain hydroxyl group hydrogen bonds with the backbone amide and side-chain carboxyl groups of Asp^{21}, and the Thr^{18} backbone amide hydrogen bonds with the Asp^{21} carboxyl group as well. On the hydrophobic face of the amphipathic p53 helix, three of the hydrophobic amino acids (Phe^{19}, Trp^{23}, Leu^{26}) have extended side-chain conformations and pack close to each other, making sequential van der Waals contacts (Fig. 4). Most noteworthy are the aromatic side chains of Phe^{19} and Trp^{23}, which stack face-to-face in a staggered arrangement (Fig. 4). The remaining two hydrophobic amino acids (Leu^{22} and Leu^{25}) have less extended side chains and do not interact with any of the others, packing instead with the body of the α helix (Fig. 4A). The two charged amino acids of the helix (Asp^{21} and Lys^{24}) are within salt bridge distance, although the amino group of the lysine is partially disordered, presumably because of the high ionic strength of the crystallization solution. Immediately after the α helix is Pro^{27}, which is likely to contribute to its termination, and Glu^{28} and Asn^{29}, which have extended backbone conformations.

In the absence of MDM2, the α helix is readily digested by proteases, including cleavage at Trp^{23} (*31*), and it is possible that it is only loosely folded, or folded in only a fraction of the molecules. Stable helix formation may thus be induced by the fitting of the hydrophobic amino acids in the cleft of MDM2.

Structure of the MDM2-p53 interface. The MDM2 cleft is lined with 14 conserved hydrophobic and aromatic amino acids that make multiple van der Waals contacts to p53 (Met^{50}, Leu^{54}, Leu^{57}, Gly^{58}, Ile^{61}, and Met^{62} from the α2 helix, Tyr^{67}, His^{73}, Val^{75}, Phe^{91}, and Val^{93} from the middle β sheet, and His^{96}, Ile^{99}, and Tyr^{100} from the α2′ helix, Fig. 4). The p53 helix binds at the entrance of the cleft, packing, on one side, with the α2 helix of MDM2 in an antiparallel orientation and, on the other side, with the ends of the MDM2 middle β sheet (Fig. 4). The β sheet ends contain reverse turns (two turns between β3 and β1′ and one between β2′ and α2′) and they provide a rigid surface on which the p53 helix packs (Fig. 4B). The position of the p53 helix allows Phe^{19}, Trp^{23}, and Leu^{26}, which are aligned along its hydrophobic face, to insert deep inside the MDM2 cleft (Fig. 5A), and pack with the cleft in a complementary fashion (Fig. 5B). The closest approach at the interface occurs between Phe^{19} and Trp^{23} of PS3 and the body of the α2 helix of MDM2. Phe^{19} makes van der Waals contacts to Ile^{61} and Gly^{58} of MDM2, while Trp^{23} makes van der Waals contacts to Gly^{58} and Ile^{61} (Fig. 4). Additional van der Waals contacts are provided by Leu^{22} of p53, which packs against the side of the MDM2 cleft (β sheet).

After the α helix, the extended region of p53 (residues 27 to 29) packs against the shallow end of the MDM2 cleft (Figs. 4 and 5A). There are only a few van der Waals contacts in this region, and they primarily involve the Pro^{19} side chain of p53. The COOH-terminal Glu^{28} and Asn^{29} residues also pack against MDM2, but they are partially disordered, and we presume that they do not contribute significantly to binding.

The p53-MDM2 interface buries 1498 $Å^2$ of surface area, most of which is hydrophobic. The van der Waals contacts at the interface are augmented by only two intermolecular hydrogen bonds: one between the Phe^{19} backbone amide of p53 and the Gln^{72} side chain of MDM2 at the entrance of the cleft (Fig. 4), and another between the p53 Trp^{23} indole group and the MDM2 Leu^{54} backbone carbonyl deep inside the cleft (Fig. 4).

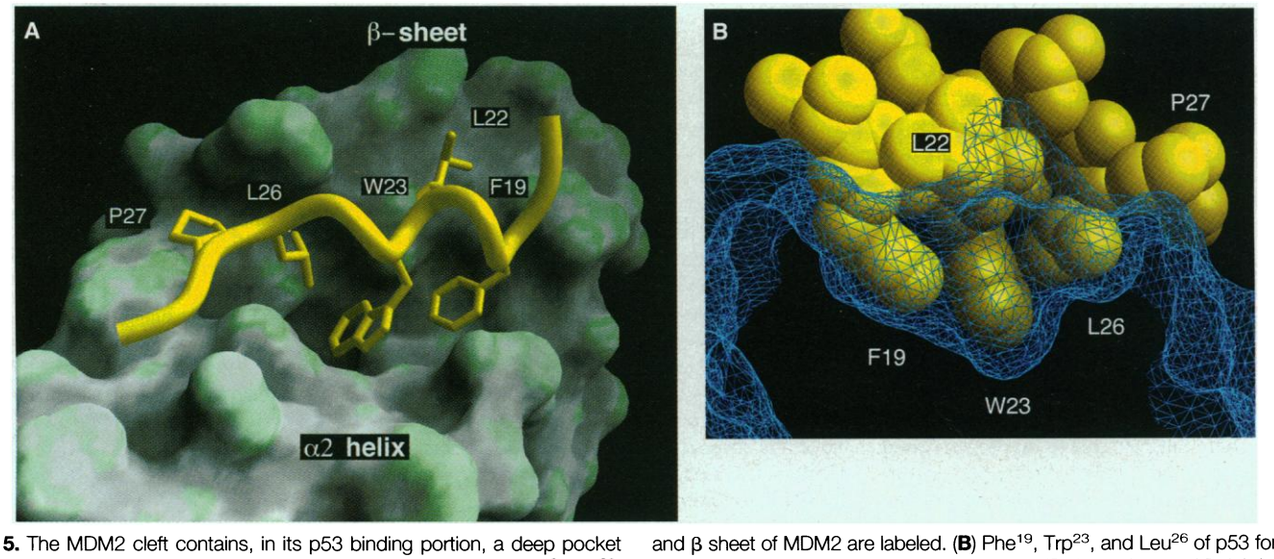

Fig. 5. The MDM2 cleft contains, in its p53 binding portion, a deep pocket where a triad of hydrophobic and aromatic p53 amino acids—Phe^{19}, Trp^{23}, and Leu^{26}—insert into. (**A**) Surface representation of the MDM2 cleft with gray concave regions highlighting its pocket-like characteristics. The p53 amino acids that interact with this surface are shown in yellow, and are labeled. Orientation is similar to Fig. 2A and the regions corresponding to the α2 helix and β sheet of MDM2 are labeled. (**B**) Phe^{19}, Trp^{23}, and Leu^{26} of p53 form a structure that is highly complementary to the MDM2 pocket, and fit tightly in it. A cross section of the interface showing the complementarity of p53 with the MDM2 pocket. The MDM2 surface is represented as a blue wire mesh and p53 residues 18 to 27 are in space filling representation. The orientation is similar to that of Fig. 4B [prepared with the program GRASP (*52*)].

The key role the hydrophobic residues play at the interface is supported by the mutational analysis of the p53 NH_2-terminus where a double mutation at the Leu^{22}-Trp^{23} sequence eliminated MDM2 binding (*24*). Furthermore, a systematic study with short peptides identified alanine mutations at Phe^{19}, Leu^{22}, and Trp^{23} as being the most disruptive to MDM2 binding (*25*). That study showed that mutation of Asp^{21} also disrupted binding. Asp^{21} does not contact MDM2 in the crystal structure, and we presume that its substitution by alanine destabilizes the α helix because of the partial loss of the amphipathic nature, as well as the elimination of the Asp^{21}-Thr^{18} hydrogen bond network which helps initiate the helix.

Implications for understanding the protein binding activity of MDM2. Recent studies have identified the E2F1-DP1 transcription factor complex (*32*), and the retinoblastoma (Rb) protein (*33*) as additional targets of the protein binding activity of MDM2, and have suggested a broader role for MDM2 in modulating cell growth controls. The NH_2-terminal structural domain of MDM2 is also the binding site for the E2F1 transcription factor (*32*), whereas the MDM2 region responsible for Rb binding has not yet been delineated. E2F1 contains a region homologous to the MDM2 binding portion of p53, having a similar pattern of hydrophobic amino acids (D*F*S*G*L*L*PEE of E2F1 compared to T*F*S*D*L*W*KLL of p53, with the homologous hydrophobic residues in italics), and a double mutation at the Asp-Phe sequence in this region of E2F1 eliminates MDM2 binding. These observations suggest that the E2F1-MDM2 and p53-MDM2 interfaces may have common structural elements. Nevertheless, there are likely to be differences in the two complexes because Leu^{26} of p53, which makes key contacts to hydrophobic MDM2 residues, is replaced by a glutamic acid in E2F1.

From a structural perspective, the MDM2-p53 complex differs from most other protein-peptide complexes characterized so far because the interface relies primarily on van der Waals contacts and the buried surface area is nearly all hydrophobic. In most other protein-peptide complexes, including those of MHC class I (*34*) and II (*35*) molecules, antibodies (*36*), and SH2 and SH3 domains (*37*), and calmodulin (*38*), there are extensive hydrogen bond contacts that are likely to contribute significantly to binding, and a significant portion of the buried surface area in those complexes is polar (*34*–*38*).

The differences in the nature of intermolecular contacts may be related to differences in the functions of the various peptide binding proteins structurally characterized to date. For example, MHC molecules (*34, 35*), calmodulin (*38*), SH2 and SH3 domains (*37, 39*) need the capacity to bind peptides having significant sequence diversity, whereas MDM2 appears to have a higher degree of specificity for a smaller set of targets, which to date includes p53 and E2F1.

Conversely, a similarity between MDM2 and several other peptide binding proteins, including MHC molecules (*34, 35*), calmodulin (*38*), and antibodies (*36*), is that they all have twofold pseudosymmetry and their peptide binding clefts occur at the interface of their pseudosymmetry-related domains. This shared feature points to intramolecular dimerization, or intermolecular dimerization in the case of antibodies, as a common path for the evolution of peptide binding clefts.

Implications for understanding transactivation domain function. MDM2 binding and activation of transcription by p53 appear to require similar, or overlapping, sets of p53 residues because multiple mutations in the hydrophobic amino acids that contact MDM2 in the crystal structure (Phe^{19}, Leu^{22}, Trp^{23} and Leu^{26}) also reduce or eliminate transactivation (*24, 40*), whereas mutations in polar or charged amino acids, either in the helix or in the flanking regions, in general have little or no effect (*24, 40*). Furthermore, studies of p53 binding to TAFs, which have emerged as the primary targets of transactivation domains (*41*), have shown that the L22Q–W23S double mutation on the hydrophobic face of the helix eliminates the physical interaction between p53 and the TAF31-TAF80 complex (*30*). These data support the model that the transactivation domain of p53 may transactivate as an amphipathic α helix, with its hydrophobic residues contacting the TAF complex (although a contribution to transactivation from sequences flanking the amphipathic helix cannot be excluded).

An amphipathic α-helical structure is compatible with sequences present in the transactivation domains of several other transcription factors (*42*), and there is a body of mutational evidence indicating that hydrophobic amino acids in these putative amphipathic α helices play an important role in transactivation (*42, 43*). A comparison of the putative helical regions from several transactivation domains (*42*) with the α helix of p53 shows that the bulky hydrophobic amino acids of p53 that contact MDM2, and are likely to also contact the TAFs, are generally conserved, and that the Thr^{18}-Asp^{21} pair of p53, which helps initiate the helix, is often replaced by amino acids that can serve in analogous roles (Asp or Pro for Thr^{18} and Ser for Asp^{21}). In several transactivation domains, the amphipathic pattern is disrupted by single amino acid insertions or deletions, but it is possible that the phase of the helix can be adjusted by an interconversion between α- and 3_{10}-helical forms and maintain its amphipathic character. These observations suggest that the amphipathic helix may be a common structural motif used in TAF binding and transactivation.

The pattern of hydrophobic residues may thus be a more useful parameter than the acidity, proline, or glutamine content commonly used for the classification of transactivation domains (*42*). In this respect, the NFkB transcription factor, which has a hydrophobic amino acid pattern that is very similar to that of p53 (D*F*SA*LL*S-Q*I*S of NFkB compared to T*F*SD*L*W*KLL*P of p53, where the conserved hydrophobic amino acids are in italics), also targets the TAF31-TAF80 complex (*44*). However, not all transactivation domain sequences are consistent with an amphipathic helix structure, and it is likely that other structural motifs may be used, especially with transcription factors that bind TAFs other than the TAF31-TAF80 complex.

The principal finding that emerges from our study is that the primary contacts to MDM2 are made by three hydrophobic and aromatic p53 amino acids which, packing together, form a structure that is complementary to and fills up a hydrophobic pocket of MDM2 (Fig. 5B). The three side chains amount to approximately 300 daltons, and this suggests that the MDM2 pocket may be a suitable binding site for small-molecule compounds. The crystal structure thus provides a framework for the discovery of compounds that may prevent the inactivation of the p53 tumor suppressor by the MDM2 oncogene in cancer.

REFERENCES AND NOTES

1. L. R. Livingstone *et al.*, *Cell* **70**, 923 (1992); Y. Yin, M. A. Tainsky, F. Z. Bischoff, L. C. Strong, G. M. Wahl, *ibid.*, p. 937; M. B. Kastan *et al.*, *Cell* **71**, 587 (1992); S. M. Cross *et al.*, *Science* **267**, 1353 (1995).
2. H. Symonds *et al.*, *Cell* **78**, 703 (1994); C. Caelles, A. Heimberg, M. Karin, *Nature* **370**, 220 (1994); X. Wu and A. J. Levine, *Proc. Natl. Acad. Sci. U.S.A.* **91**, 3602 (1994); H. Hermeking and D. Eick, *Science* **265**, 2091 (1994); P. Sabbatini, J. Lin, A. J. Levine, E. White, *Genes Dev.* **9**, 2184 (1995).
3. A. J. Levine, J. Momand, C. A. Finlay, *Nature* **351**, 453 (1991); B. Vogelstein and K. W. Kinzer, *Cell* **70**, 523 (1992); L. J. Ko and C. Prives, *Genes Dev.* **10**, 1054 (1996).
4. M. S. Greenblatt, W. P. Bennett, M. Hollstein, C. C. Harris, *Cancer Res.* **54**, 4855 (1994).
5. L. Cahilly-Snyder, T. Yang-Feng, U. Francke, D. L. George, *Somat. Cell Mol. Genet.* **13**, 235 (1987).
6. J. Momand, G. P. Zambetti, D. C. Olson, D. George, A. J. Levine, *Cell* **69**, 1237 (1992).
7. J. D. Oliner, K. W. Kinzler, P. S. Meltzer, D. L. George, B. Vogelstein, *Nature* **358**, 80 (1992).
8. J. P. Bargonetti, N. Friedman, S. E. Kern, B. Vogelstein, C. Prives, *Cell* **65**, 1083 (1991); S. E. Kern *et al.*, *Science* **252**, 1708 (1991); W. S. El-Deiry, S. E. Kinzler, J. A. Pietenpol, K. W. Kinzler, B. Vogelstein, *Nature Genet.* **1**, 45 (1992).
9. S. Fields and S. K. Jang, *Science* **249**, 1046 (1990);

L. Raycroft, H. Wu, G. Lozano, *ibid.*, p. 1049; G. Farmer *et al.*, *Nature* **358**, 83 (1992); S. E. Kern *et al.*, *Science* **256**, 827 (1992).
10. J. A. Pietenpol *et al.*, *Proc. Natl. Acad. Sci. U.S.A.* **91**, 1998 (1994).
11. X. Wu, J. H. Bayle, D. Olson, A. J. Levine, *Genes Dev.* **7**, 1126 (1993).
12. J. D. Oliner *et al.*, *Nature* **362**, 857 (1993).
13. R. M. de Oca Luna, D. S. Wagner, G. Lozano, *ibid.* **378**, 203 (1995); S. N. Jones, A. E. Roe, L. A. Donehower, A. Bradley, *ibid.*, p. 206.
14. F. S. Leach, *et al.*, *Cancer Res.* **53**, 2231 (1993); C. Cordon-Cardo *et al.*, *ibid.* **54**, 794 (1994).
15. G. Reifenberger, L. Lu, K. Ichimura, E. E. Schmidt, V. P. Collins, *ibid.* **53**, 2736 (1993).
16. C. E. Bueso-Ramos, Y. Yun, E. deLeon, P. McCowm, S. Stass, M. Albitar, *Blood* **82**, 2617 (1993).
17. I. Shibagaki *et al.*, *Clin. Cancer Res.* **1**, 769 (1995).
18. A. Marchetti *et al.*, *J. Pathol.* **175**, 31 (1995).
19. S. S. Fakharzadeh, S. P. Trusko, D. L. George, *EMBO J.* **10**, 1565 (1991).
20. C. A. Finlay, *Mol. Cell. Biol.* **13**, 301 (1993).
21. J. Chen, V. Marechal, A. J. Levine, *ibid.*, p. 4107 (1993).
22. Y. Cho, S. Gorina, P. D. Jeffrey, N. P. Pavletich, *Science* **265**, 346 (1994).
23. W. Lee, *et al. Nature Struct. Biol.* **1**, 877 (1994); P. D. Jeffrey, S. Gorina, N. P. Pavletich, *Science* **267**, 1498 (1995).
24. J. Lin, J. Chen, B. Elenbaas, A. J. Levine, *Genes Dev.* **8**, 1235 (1994).
25. S. M. Picksley, B. Vojtesek, A. Sparks, D. P. Lane, *Oncogene* **9**, 2523 (1994).
26. Digestion of the GST-MDM2 (residues 1 to 491) fusion protein by subtilisin yielded a 12-kD structural domain corresponding to residues 17 to 124 of MDM2, which, consistent with biochemical studies (*12*, *21*, *24*, *25*) has the p53-binding activity of MDM2. Proteolytic digestion with subtilisin and amino- and carboxyl-peptidases of a complex consisting of the p53 NH_2-terminal region (residues 1 to 95) bound to MDM2, coupled with a systematic screen of synthetic peptides, indicated that a p53 region as small as residues 17 to 27 retained the capacity to bind MDM2. Complexes of MDM2 with p53 peptides containing this region do not dissociate detectably during gel filtration chromatography, indicating a long half-life association.
27. The NH_2-terminal domain of human MDM2, corresponding to amino acids 17 to 125, was overexpressed in *E. coli* from the pET3d expression vector at 20°C, and was purified by cation exchange chromatography. The p53 peptide, corresponding to amino acids 15 to 29 of human p53, was chemically synthesized and then purified by reversed phase chromatography. The complex was prepared by mixing a solution of the MDM2 domain (1 mM) with a twofold molar excess of the p53 peptide; the product was purified by gel filtration chromatography on a Superdex75 column (Pharmacia) and concentrated to 1.5 mM by ultrafiltration in 25 mM MES (sodium salt) 250 mM NaCl, 5 mM dithiothreitol (DTT), pH 6.8. Crystals of the complex were grown by the hanging drop vapor diffusion method at 4°C from 79 percent saturated potassium phosphate, 50 mM tris-HCl, 5 mM DTT, pH 8.4. Crystals form in space group $C222_1$ (a = 43.4 Å; b = 100.5 Å; and c = 54.8 Å) and have one complex in the asymmetric unit.
28. V. Marechal *et al.* in preparation.
29. The *X. laevis* MDM2 (residues 13 to 119)–human p53 (residues 13 to 29) complex was prepared according to procedures similar to those used for the human complex. Crystals of the complex were grown at 16°C from 45 percent saturated $(NH_4)_2(SO_4)$, 100 mM tris-HCl, 5 mM DTT, pH 8.0; they form in space group $P6_322$ with (a = b = 85.0 Å, c = 63.9 Å) and have one complex in the asymmetric unit. Heavy atom soaks were performed in 60 percent saturated $(NH_4)_2(SO_4)$, 50 mM tris-HCl, 25 mM NaCl, pH 8.0, containing one of the following heavy atom solutions: 1 mM thimerosal for 7 hours, 3 mM $UO_2(OAc)_2$ for 24 hours, 1 mM $K_2Au(CN)_4$ for 12 hours, and for the doubly substituted derivative 6 mM $UO_2(OAc)_2$ for 8 hours followed by 3 mM $K_2Pt(CN)_4$ for 14 hours (platinum binding produced centrosymmetric phases; therefore a double substitution was used). Initial MIR phases calculated with the program MLPHARE (*45*) had a mean figure of merit of 0.64 to 3.0 Å, and were improved with solvent flattening and histogram matching with the program SQUASH (*46*). The MIR maps gave interpretable electron density for the entire MDM2 and p53 polypeptides of the final model. The model was built into MIR electron density maps with the program O (*47*), and was refined by simulated annealing with the program X-PLOR (*48*), and least squares refinement with TNT (*49*). The structure of the human MDM2-p53 complex was determined by molecular replacement with X-PLOR (*48*) using the *X. laevis* complex structure as the search model (correlation coefficient of 0.60 for 15.0 to 4.0 Å data), and was refined by simulated annealing and least squares refinement. The refined model contains residues 25 to 109 of human MDM2 and residues 17 to 29 of human p53. The NH_2- and COOH-terminal regions of MDM2 (residues 17 to 24 and 110 to 125) and residues 15 to 16 of p53 have no electron density in the maps, and we presume that these regions are disordered in the crystal.
30. C. J. Thut, J. Chen, R. Klemm, R. Tjian, *Science* **267**, 100 (1995); H. Lu and A. J. Levine, *Proc. Natl. Acad. Sci. U.S.A.* **92**, 5154 (1995).
31. N. P. Pavletich, K. A. Chambers, C. O. Pabo, *Genes Dev.* **7**, 2556 (1993).
32. K. Martin *et al.*, *Nature* **375**, 691 (1995).
33. Z.-X. Xiao *et al.*, *ibid.*, p. 694.
34. P. J. Bjorkman *et al.*, *ibid.* **329**, 506 (1987).
35. J. H. Brown *et al.*, *ibid.* **364**, 33 (1993).
36. I. A. Wilson, J. B. Ghiara, R. L. Stanfield, *Res. Immunol.* **145**, 73 (1994).
37. R. L. Stanfield and I. A. Wilson, *Curr. Opinion Struct. Biol.* **5**, 103 (1995).
38. W. E. Meador, A. R. Means, F. A. Quiocho, *Science* **257**, 1251 (1992).
39. G. B. Cohen, R. Ruibao, D. Baltimore, *Cell* **80**, 237 (1995).
40. J. Chang, D. Kim, S. W. Lee, K. Y. Choi, Y. C. Sung, *J. Biol. Chem.* **270**, 25014 (1995).
41. J. A. Gooodrich and R. Tjian, *Curr. Opinion Cell Biol.* **6**, 403 (1994); S. K. Burley and R. G. Roeder, *Annu. Rev. Biochem.* **65**, 769 (1995).
42. W. D. Cress and S. J. Triezenberg, *Science* **251**, 87 (1991); M. L. Schmitz *et al.*, *J. Biol. Chem.* **269**, 25613 (1994); S. J. Triezenberg, *Curr. Opinion Genet. Dev.* **5**, 190 (1995); M. E. Massari, P. A. Jennings, C. Murre, *Mol. Cell. Biol.* **16**, 121 (1996).
43. J. L. Reiger, F. Shen, S. J. Triezenberg, *Proc. Natl. Acad. Sci. U.S.A.* **90**, 883 (1993); W. S. Blair, H. P. Bogerd, B. R. Cullen, *J. Virol.* **68**, 3803 (1994); W. S. Blair, H. P. Bogerd, S. J. Madore, B. R. Cullen, *Mol. Cell. Biol.* **14**, 7226 (1994); M. Tanaka and W. Herr, *ibid.* **14**, 6056 (1994); G. Gill, E. Pascal, Z. H. Tseng, R. Tjian, *Proc. Natl. Acad. Sci. U.S.A.* **91**, 192 (1994).
44. X. Xialoing *et al.*, *Nature* **380**, 316 (1996).
45. Collaborative Computational Project, No. 4. *Acta Crystallogr.* **D50**, 760 (1994).
46. K. Y. J. Zhang, *Acta Crystallogr.* **D49**, 213 (1993).
47. T. A. Jones, J.-Y. Zou, S .W. Cowan, *Acta Crystallogr.* **A47**, 110 (1991).
48. A. T. Brunger, *X-PLOR, a system for crystallography and NMR, Version 3.0 Manual* (Yale Univ. Press, New Haven, CT 1991).
49. D. E. Tonrud, L. F. Ten Eyck, B. W. Matthews, *Acta Crystallogr.* **A43**, 489 (1987).
50. P. J. Kraulis, *J. Appl. Crystallogr.* **24**, 946 (1991).
51. E. A. Merrit and M. E. Murphy, *Acta Crystallogr.* **D50**, 869 (1994).
52. A. Nicholls, and K. A. Sharp, B. Honig, *Proteins: Struct. Funct. Genet.* **11**, 281 (1991).
53. We thank S. Geromanos of the Sloan-Kettering Microchemistry Facility for peptide synthesis, NH_2-terminal sequence and mass spectroscopic analyses; P. D. Jeffrey for helpful discussions; and R. Kenny for administrative help. Supported by the NIH (CA65698), the Pew Charitable Trusts, the Arnold and Mabel Beckman Foundation, the Dewitt Wallace Foundation, and the Samuel and May Rudin Foundation. Coordinates have been deposited with the Brookhaven Protein Data Bank (1YCQ and 1YCR).

11 July 1996; accepted 24 September 1996